Correlation between 2D and 3D flow curve modelling of DP steels using a microstructure-based RVE approach

A. Ramazani *, K. Mukherjee, H. Quade, U. Prahl, W. Bleck

Department of Ferrous Metallurgy, RWTH Aachen University, Intzestr.1, D-52072 Aachen, Germany

ABSTRACT

A microstructure-based approach by means of representative volume elements (RVEs) is employed to evaluate the flow curve of DP steels using virtual tensile tests. Microstructures with different martensite fractions and morphologies are studied in two- and three-dimensional approaches. Micro sections of DP microstructures with various amounts of martensite have been converted to 2D RVEs, while 3D RVEs were constructed statistically with randomly distributed phases. A dislocation-based model is used to describe the flow curve of each ferrite and martensite phase separately as a function of carbon partitioning and microstructural features. Numerical tensile tests of RVE were carried out using the ABAQUS/Standard code to predict the flow behaviour of DP steels. It is observed that 2D plane strain modelling gives an underpredicted flow curve for DP steels, while the 3D modelling gives a quantitatively reasonable description of flow curve in comparison to the experimental data. In this work, a von Mises stress correlation factor σ_{3D}/σ_{2D} has been identified to compare the predicted flow curves of these two dimensionalities showing a third order polynomial relation with respect to martensite fraction and a second order polynomial relation with respect to equivalent plastic strain, respectively. The quantification of this polynomial correlation factor is performed based on laboratory-annealed DP600 chemistry with varying martensite content and it is validated for industrially produced DP qualities with various chemistry, strength level and martensite fraction.

© 2012 Elsevier B.V. All rights reserved.

1. Introduction

Recent studies have shown that in future cars DP steels can occupy up to 80% of the total weight of the car. For instance, DP600 is used in the dash cross member, B-pillar and front rail closeout [1–5]. The reason is that DP steels offer an outstanding combination of strength and ductility due to their microstructure, in which a hard martensitic phase is dispersed in a soft ferrite phase [6–10]. The flow behaviour of DP steel depends not only on the properties of ferrite and martensite, but also on the microstructural features such as volume fraction and morphology of martensite islands [11–14]. In DP steels, the strength of ferrite can be estimated by its composition and grain size [15–17]. The ferrite phase also gets additional strength from the initial dislocation density due to austenite to martensite transformation during cooling [18–20]. The strength of martensite depends primarily on its carbon content showing a linear increase of yield strength by increasing (local) carbon content [11,21]. According to Leslie, with the increase of the carbon content in martensite from 0.2 to 0.3 wt%, the yield stress increases linearly from 1000

to 1265 MPa. The substitutional alloying elements Mn, Si, etc. also strengthen the martensite, but their effect is secondary compared to the effect of the carbon content.

The modelling of mechanical properties of DP steels can be divided into two categories. One of them considers the constitutive laws as that of a single constituent. The other considers the laws to be a function of the independent constitutive laws of ferrite and martensite. Khan et al. [22] have successfully modelled the quasistatic and dynamic responses of DP steels using the modified Khan–Huang–Liang (KHL) model. The modified KHL model was used to predict the flow stress as a function of plastic strain of the DP steel [22–25].

Many researchers are currently focusing on building models to predict the flow behaviour of DP steels from their microstructure [26–33]. 2D microstructure modelling based on plane strain or axisymmetric cell models reduces the complexity of 3D modelling and minimises the computational cost. Although on a different material, the research of Ghosh et al. [34] has shown that RVE modelling of materials containing heterogeneities can provide essential inputs to a homogenisation-based continuum plasticity-damage model for ductile failure.

Several authors have introduced the concept of 2D RVE modelling in which the finite element mesh is generated from real microstructure [26–28]. Asgari et al. used a specialised microstructural

* Corresponding author. Tel.: +49 241 80 95841; fax: +49 241 80 92253.
E-mail address: ali.ramazani@iehk.rwth-aachen.de (A. Ramazani).

meshing program OOF (Object Oriented Finite element analysis software [35]) to generate 2D RVE based on DP real micrographs [26]. In a former study, light optical microscopy (LOM) images of real microstructures were converted into 2D RVE models by using an in-house program, Gitter, with regard to the colour difference of martensite and ferrite after etching [27]. The effect of microstructural morphology on the mechanical behaviour has been studied for DP steels, since the generated RVE from the real microstructure was able to involve the morphology effect on the predicted flow curves. 2D RVE modelling has been employed not only in DP steel but in other multiphase materials also and significant findings have been published, which can be of relevance for DP steel research also. For example, Xia and Wang [36] worked on dual-phase composites and proposed that the toughening behaviour of these kinds of materials is due to the propagation and multiplication of localised deformation bands. Lim et al. [37] proposed a dislocation interaction-based model to simulate polycrystal deformation with grain and grain boundary effects. Srivastava and Weng [38] noted the similarities between the extensions from linear piezoelectricity to nonlinear ferroelectricity and from linear elasticity to nonlinear plasticity and have shown the influence of a compressive stress on the nonlinear response of ferroelectric crystals.

Recently, several researchers have focussed on being able to predict the formability and failure behaviour of DP steels based on 2D RVE modelling. Kim et al. [39] have modelled the hole-expansion formability of DP steels using an RVE-based FEM approach. This study utilised Ludwik's equation to model the flow curves of individual ferrite and martensite phases. Sun et al. [40] created 2D RVE from real DP steel microstructures and modelled the flow curves and failures of these types of steel. Their study was successful in predicting the failure modes and ductility of DP steels through plastic strain localisation. This study utilised Ludwik's equation to model the flow curves of individual ferrite and martensite phases. The term "micromechanical modelling" has been coined for this type of modelling where the mechanical properties of the composite phase are determined by taking into consideration the real microstructure and the flow behaviour of the microstructural constituents.

Nevertheless, the 2D approach gives rise to some criticism because the real specimen deforms 3D. For example Thomser indicated that the flow curves predicted from 2D plane strain modelling underestimates the experimentally obtained flow curves [41].

In order to improve reality in the modelling, 2D RVE has been extended towards simplified 3D [42–46]. Since Tvergaard [42] introduced his stacked hexagonal array (SHA) model, several researchers have utilised it to model heterogeneous materials. Comparing experimental and modelling studies have shown that the distribution of the phases strongly affects the macroscopic material response due to the localisation, which arises in the matrix. Huang and Kinloch [44] and Danielsson et al. [45] used an idealised approach based on plane strain and axisymmetric models. However, the models based on the plane strain idealisation were shown to be unable to represent or capture the mechanical behaviour of DP steels, especially at a high volume fraction of martensite (V_m). Alabbasi [47] used the micromechanical approach based on the SHA model and showed that this model could well represent DP steel as it displays an intrinsic ability to capture the expected stress–strain behaviour with increasing V_m and in terms of deformation fields of the constituents. Alabbasi [47] used plain strain material idealisations of simple square array, staggered square array and stacked hexagonal array. For the axisymmetric SHA model, Al-Abbasi reported that the 2D plane strain model overpredicts strain hardening, which gives rise to fictitious suppression of localisation. They made the observation that in plane strain models, the martensite remains elastic,

but in the SHA model, the martensite shows some plastic strain. They concluded that plastic deformation of martensite is an important matter to be captured in the micromechanical modelling of DP steel and SHA modelling is capable of taking into account the plastic deformation of martensite. These results are in agreement with the experimental results of Calcagnotto et al. [48], which report that martensite deforms plastically during the tensile test of DP steels. An alternative approach for the definition of 3D RVE has been applied by Iung and Grange using a simplified cubic 3D calculation framework in FEM to model the mechanical behaviour of an ideal two-phase (a hard phase and a soft phase) material [49]. They varied the volume fraction of the hard and soft phases by labelling the elements randomly as either hard or soft phases. They implemented the boundary conditions in such a fashion that the macroscopic shear introduced to the structure is zero.

Several researchers have emphasised that instead of geometrically simplified cellular representation, a full 3D FEM simulation of more realistic microstructures is needed to improve the simulation quality of mechanical behaviour of two-phase materials [47,50–57]. The simplest assumption for a two-phase microstructure with spherical second phase inclusions in a surrounding matrix is that the second phase distribution is homogenous, periodic and globular. The classical Mori–Tanaka approach [57] is based on these assumptions. Kaluza [56] introduced a statistical procedure in order to study the mechanical properties of quasi-brittle heterogeneous materials based on a cube of regularly meshed 10-node-tetrahedron elements. The second phase particle was built up by an arrangement of elements that have the shape of a tetrakai-decahedron.

Uthaisangsuk has created real 3D RVEs slice wise from optical micrographs. For this purpose, he took optical micrographs of DP steel at a depth of 6 µm consecutively and from 8 such micrographs he created a 3D RVE using brick elements (C3D8) to reconstruct the 3D RVE from the micrographs' sections [55]. Lewis et al. used EBSD to recreate a 3D microstructure of austenitic steel by serial sectioning of consecutive planes. An alternative approach has been represented by Rudnizki through the process modelling of a microstructure evolution to generate a statistical representative RVE description. State of the art phase field software MICRESS has been used to model the microstructure evolution during intercritical annealing of cold-rolled DP steel and to predict final phase fractions and grain size distribution realistically [58]. Kim et al. [59] performed a crystal plasticity-based multi-scale micromechanical modelling to predict the Bauschinger effect in DP steels. 3D RVE modelling has been employed not only in DP steel but also in other multiphase materials and significant findings have been published, which can also be of relevance for DP steel research. For instance, Mayeur and McDowell [60] developed a 3D crystal plasticity model for duplex Ti–6Al–4V.

Since in the above-mentioned approaches the 3D RVE is constructed with homogeneous distribution of ferrite and martensite, effects of microstructural inhomogeneities (e.g. banding) have not been taken into account, while the 2D approach using real micrographs for RVE construction easily takes into account such effects. Nevertheless, the specimen deforms three-dimensionally and a 2D model just satisfies a simplification assumption, e.g. plane strain. Besides, the major advantage of 2D calculations is that the calculation takes less time than 3D calculations.

The current study aims to study the effect of dimensionality in the micromechanical modelling of DP steels with homogeneous distributed martensite islands. Hence, an attempt has been made to compare the flow curves of DP steels obtained from experiments and both 2D plane strain and 3D calculations. Several DP microstructures with varying martensite fraction were created by controlling the heat-treatment parameters. Two in-house programs

Table 2.1.1
Chemical composition of the investigated DP steels (in wt%).

	C	Si	Mn	P	S	Cr	Ni	Al	Cu	V
DP500	0.071	0.096	1.42	0.016	0.001	0.48	0.023	0.034	0.013	0.007
DP600	0.072	0.25	1.58	0.015	0.001	0.055	0.024	0.032	0.010	0.011
DP800	0.116	0.23	1.41	0.013	0.001	0.020	0.034	0.032	0.006	0.017
DP1000	0.142	0.53	1.40	0.009	0.002	0.016	0.03	0.039	0.02	0.008
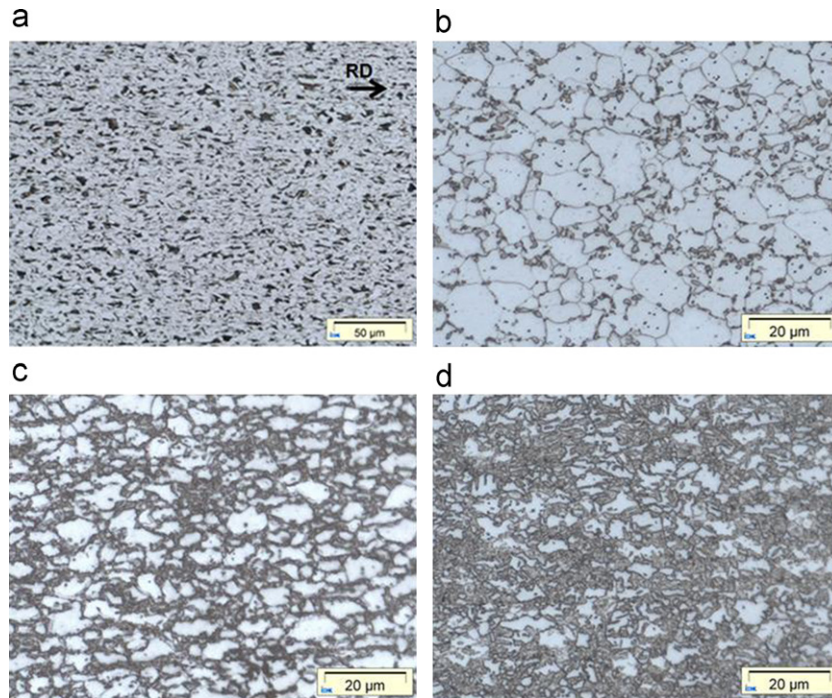
Fig. 2.1.1. As received, microstructures of various DP qualities: (a) cold-rolled DP600, (b) DP500, (c) DP800 and (d) DP1000 steels.

were employed to generate 2D and 3D RVEs. The experimental results were compared with the predicted results. The calculated yield stress using 2D modelling correlates to the estimated yield stress from 3D simulation through a 2D/3D correlation factor, which is a polynomial relation with respect to martensite fraction and equivalent plastic strain.

2. Experimental

2.1. Materials

In this study, four DP qualities were investigated following a two-step procedure. First, several martensite fractions were laboratory processed using DP600 chemistry. Based on these specimens, the 2D/3D correlation function was generated numerically. In the second step, this correlation factor was validated against three industrially produced DP qualities with different strength level and microstructure. The chemical composition of all four DP qualities is given in Table 2.1.1. The delivered microstructures of the steels are shown in Fig. 2.1.1.

For the first step, DP microstructures were produced from a DP600 steel composition that was delivered in a cold-rolled, ferrite pearlite state with a thickness of 1 mm. Here, three different martensite contents were processed by laboratory heat treatment.

In order to generalise the developmental approach in the current research work, three industrially produced DP steels with thickness of 1 mm and varying chemistries, martensite fractions and strength levels were selected. The designations DP500, DP800
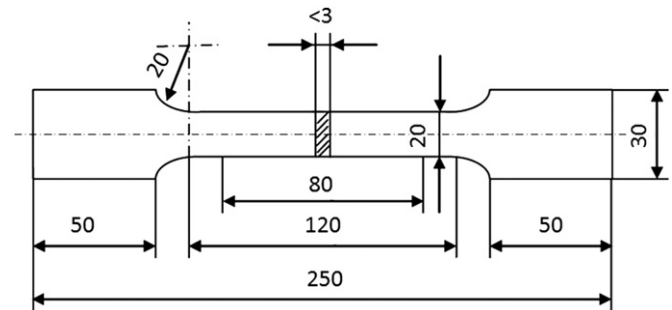

Fig. 2.3.1. Sample geometry for tensile testing (dimensions are given in mm).

and DP1000 indicate DP steels with UTS of 500, 800 and 1000 MPa, respectively. Compared to the DP600 chemistry used in the first step, these three chemistries have varying C, Mn, Si and Cr content.

2.2. Laboratory heat treatment of DP600

Laboratory heat treatment of DP600 quality was performed aiming to create DP steels with varying martensite/ferrite fraction and ferrite grain size. Sheet samples were immersed in a salt bath at three different temperatures: 740, 760 and 780 °C with a holding time of 5 min each. Finally, the samples were quenched in water to room temperature, which leads to the transformation of austenite to martensite.
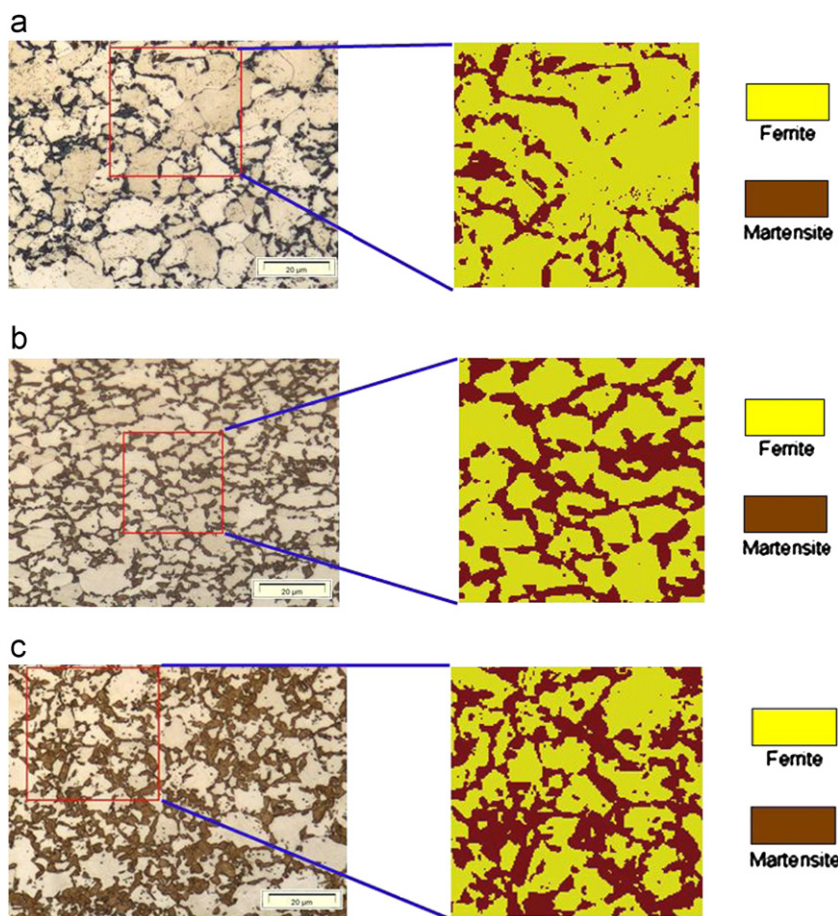
Fig. 3.1.1. Selection of 2D RVE for micromechanical modelling of DP steel with (a) 20%, (b) 37% and (c) 46% martensite.

2.3. Mechanical testing

After annealing of DP600 in salt bath or even from the delivered sheets of DP500, DP800 and DP100, tensile samples were cut from the sheet according to DIN EN 10002. The sample geometry used for mechanical testing is shown in Fig. 2.3.1. The tensile tests were performed parallel to the cold-rolling direction at a velocity of 4 mm/min at the Zwick 100. For every condition, three parallel tests were carried out.

2.4. Microstructural analysis

Quantification of microstructures was carried out by standard metallographic procedures. The samples were etched by 3% Nital. The metallographic pictures were captured from the thickness direction. For each annealing condition, 9 images were analysed. The digital images from the optical microscope were converted into a black and white image by means of a grey scale threshold binarisation (ferrite-white, martensite-black). The ferrite grain size was determined through linear intercept method (ASTM Standard E 112) and the martensite fraction was determined by quantifying the area fraction of dark areas.

2.5. Quantification of carbon partitioning

The carbon contents of ferrite (c_α) were approximated to be the equilibrium carbon content at the peak annealing temperatures. This was derived from ThermoCalc utilising the TCFe6 database. An alternative approach could be to take into account the kinetics by using DICTRA. But as not for all materials under investigation the process

parameters are known the ThermoCalc approach was used to ensure comparability for all conditions. The following elements have been taken into account for ThermoCalc calculations: Mn, C, Si, Cr and Ni. For obtaining c_α, the equilibrium iron–carbon phase diagram was calculated using the TCFe6 database taking into consideration the Mn, Si, Cr and Ni content of the steel. From the ferrite/ferrite+austenite phase boundary in the iron–carbon phase diagram, the carbon content in ferrite was determined for the responsible annealing temperature. As the ferrite/ferrite+austenite boundary in the iron–carbon phase diagram is a unique line, one single value of carbon content in ferrite was obtained for each annealing temperature. The carbon content of the martensite (c_m) phase was then calculated by considering the carbon mass balance, as shown in Eq. (2.1).

$$C_{DP} = V_m c_m + V_\alpha c_\alpha, \tag{2.1}$$

where C_{DP} is the nominal carbon composition of the DP steel.

3. Micromechanical modelling

Micromechanical modelling using numerical tensile test of a representative volume element (RVE) is an appropriate procedure to study and model the flow behaviour of DP steels. This method is advantageous since it provides a good description of the deformation of the material on the micro level giving insight into the stress and strain evolution and distribution in and between the phases.

An RVE has to be constructed in such a way that the shape, morphology, size and randomness of constituent phases can be considered to be representative of the microstructure under consideration. Hence, it should be sufficiently large to include
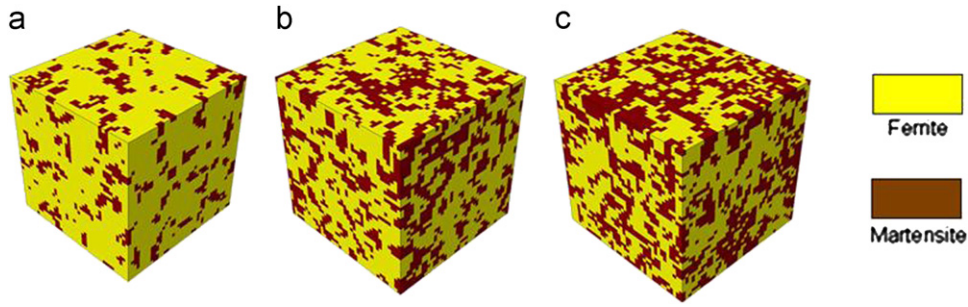
Fig. 3.1.2. 3D RVE of DP steel with (a) 20% (b) 37% and (c) 46% martensite.

the microstructural characteristics but also adequately small to optimise time expenditure for calculation. Besides the optimal size, four basic features have to be discussed to define a micro-mechanical model for multiphase material:

(a). Geometric definition of a representative volume element (RVE), which represents the vital features of the microstructure. Here, two approaches are under investigation: 2D microsection based and 3D statistically based, which will be presented in detail in the following Section 3.1.
(b). Constitutive description of the flow behaviour of each phase. Therefore, a single phase flow law is formulated based on dislocation theory and will be discussed in Section 3.2.
(c). Boundary conditions imposing the loading from macroscale. In this study, periodic boundary conditions were employed on the 2D and 3D RVEs through a developed FORTRAN program representing uniaxial numerical tensile test.
(d). Homogenisation strategy needed to represent the macroscopic mechanical behaviour from the results of the RVE's numerical evaluation. A computational first-order homogenisation by volume averaging was employed to obtain the true stress–true strain graph from the RVE calculations where the true plastic strain and stress of the RVE were assumed to be the mean of these values at each node [47,61]. After determining the flow curve from the numerical tensile test, the yield strength is determined as 0.2% offset yield strength.

3.1. RVE generation

3.1.1. 2D microsection-based RVE generation

In a former study, the acceptable size of the RVE was considered as a minimum of 24 μm while it should include at least 19 martensite particles [27]. According to this approach, the 2D RVEs from the real microstructures of DP steels with 20%, 37% and 46% martensite were created. By distinguishing bright and dark areas, LOM images of real microstructures were transformed into 2D RVE models by means of an in-house Finite Element generator, Gitter. As the dimension of RVE is small against the thickness of sheets, plane strain elements were employed in this study (CPE4R).

Additionally, the effect of mesh size was studied in a pre-study with ranging element length from 0.1 to 2 μm., and no deviation was obtained for the meshes finer than 0.25 μm. Therefore, in the current study, quadratic meshes with element size of 0.25 μm and edge length 25 μm were used for 2D modelling. The generated RVEs are shown in Fig. 3.1.1. Using an 8-core machine, the 2D RVE calculations took approximately 30 min.

3.1.2. 3D statically based RVE generation

Generally, 2D RVE has to satisfy a continuum mechanical simplification, e.g. plane strain condition, while 3D offers more reality in the plastic flow modelling. The introduced RVE is constructed statistically with random distribution of phases. The 3D RVE is cubic with dimensions of 25 μm × 25 μm × 25 μm, with an element size of 0.25 μm. The element was a hexahedron (C3D4) with a linear shape function. For the generation of a 3D DP microstructure mesh, an in-house software program was developed, which distributes the martensite inclusions randomly. The generated 3D RVEs for DP steel microstructures with (a) 20%, (b) 37% and (c) 46% martensite are depicted in Fig. 3.1.2. These calculations took a time of 240 min under a usage of 8 cores.

3.2. Single phase flow curve modelling

Few models have been described in the literature to quantify the constitutive behaviour of single phases. Of note is the dislocation density-based single-crystal constitutive equation as discussed by Lee et al. [62]. They quantified the flow resistance on a slip plane taking into account the Burger's vector, line direction and density of dislocations on all other slip planes.

In the current work, the elastic modulus for ferrite and martensite is assumed to be 210 GPa. The flow curve of individual phases for ferrite and martensite at room temperature is quantified based on a dislocation-based strain hardening model [63]. This model emerges from the classical dislocation theory approach of [64] and [65] and from the work of [66]. The model constants are quantified by [28,63] and are reported in Eqs (3.1) and (3.2).

$$\sigma \ (\text{in MPa}) = \sigma_0 + \Delta\sigma + \alpha M \mu \sqrt{b} \sqrt{\frac{1 - \exp(-M k_r \varepsilon)}{k_r L}}, \qquad (3.1)$$

where σ and ε are responsible for the flow stress (von Mises stress) and true strain (equivalent plastic strain), respectively. The description of each term in Eq. (3.1) is given below and the values used were found from an earlier work [67]. The first term σ_0 takes care of the Peierls stress and effects of alloying elements in the solid solution.

$$\begin{aligned} \sigma_0 \ (\text{in MPa}) = \ & 77 + 750(\%P) + 60(\%Si) + 80(\%Cu) \\ & + 45(\%Ni) + 60(\%Cr) + 80(\%Mn) \\ & + 11(\%Mo) + 5000(\%N_{ss}) \end{aligned} \qquad (3.2)$$

The second term, $\Delta\sigma$, provides strengthening by precipitation or the carbon in solution. In case of ferrite it is

$$\Delta\sigma \ (\text{in MPa}) = 5000(\%C_{ss}^f), \qquad (3.3)$$

while for martensite it is

$$\Delta\sigma \ (\text{in MPa}) = 3065(\%C_{ss}^m) - 161, \qquad (3.4)$$

where $\%C_{ss}^f$ and $\%C_{ss}^m$ denote the carbon content (in wt%) in ferrite and martensite, respectively.

The third term consists of the effects of dislocation strengthening as well as work softening due to recovery. α is a constant with a value of 0.33. M is the Taylor factor and a value of 3 is

Table 4.1.1
Quantification of the investigated DP steels and carbon content in ferrite and austenite at different annealing temperatures.

Material	T_A (°C)	Ferrite grain size (µm)	V_m (%)	C_α (%)	C_γ (%)
DP600	740	4.43	20	0.0066	0.334
DP600	760	3.76	37	0.0049	0.186
DP600	780	3.21	46	0.0044	0.151
DP500	760	5.42	15	0.0028	0.457
DP800	760	4.74	30	0.0037	0.378
DP1000	780	3.96	50	0.0033	0.281
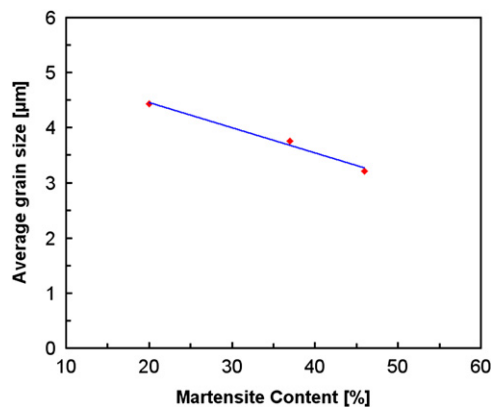
Fig. 4.1.1. Empirical relation between ferrite grain size and martensite phase fraction of the investigated DP600 steel.

utilised in this study. μ is the shear modulus and a value of 80000 MPa is used in this work. b is the Burger's vector and a value of 2.5×10^{-10} m is used in this study. k_r is the recovery rate. In the case of ferrite a value of $10^{-5}/d_\alpha$ is assumed, where d_α refers to the ferrite grain size. For martensite, the k_r value used is 41. L is the dislocation mean free path. For ferrite, it is ferrite grain size d_α, while for martensite, it is 3.8×10^{-8} m [67].

4. Results and discussions

4.1. Quantification of DP microstructures

For all investigated steel qualities, annealing temperature T_A, ferrite grain size d_α and martensite fraction V_m are summarised in Table 4.1.1 along with the carbon content in ferrite C_α and in austenite C_γ, respectively. It can be observed that with increasing UTS the carbon content of austenite at the annealing temperature is decreasing, while the amount of martensite is increasing. This increment in carbon content, which is ultimately the carbon content of the martensite islands, together with the increment in martensite fraction increases the overall strength of the DP steels. In general, there is a decrease in ferrite grain size with increasing UTS and increasing martensite content.

For the calculation of mechanical properties of single phase, carbon content and ferrite grain size are important parameters in this study. The carbon content regarding annealing temperature and ferrite grain size of DP steels with 20%, 37% and 46% were identified based on ThermoCalc calculations (see Section 2.5). In order to identify the ferrite grain size in DP600 steel with various martensite fractions, an empirical relationship between martensite fraction and ferrite grain size was introduced based on the experimental results. In Fig. 4.1.1, the ferrite grain size is plotted as a function of martensite volume fraction. From this figure, it is observed that the ferrite grain size decreases linearly with increasing martensite fraction of DP600 steel [41,68].
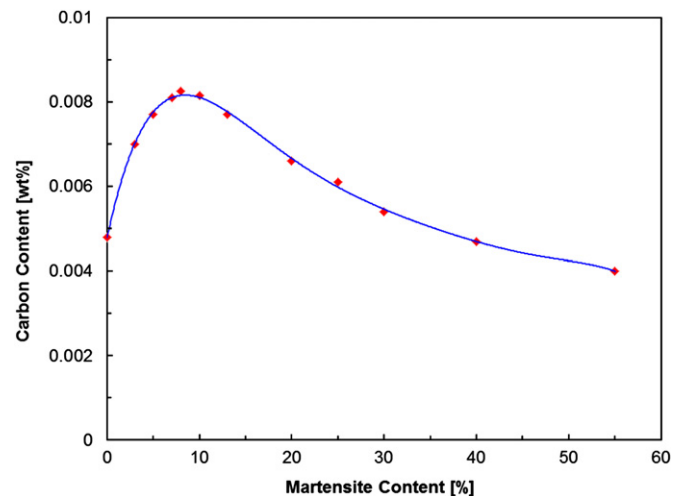
Fig. 4.1.2. Relation between the carbon content in ferrite with the volume fraction of martensite in DP600 steel under consideration.
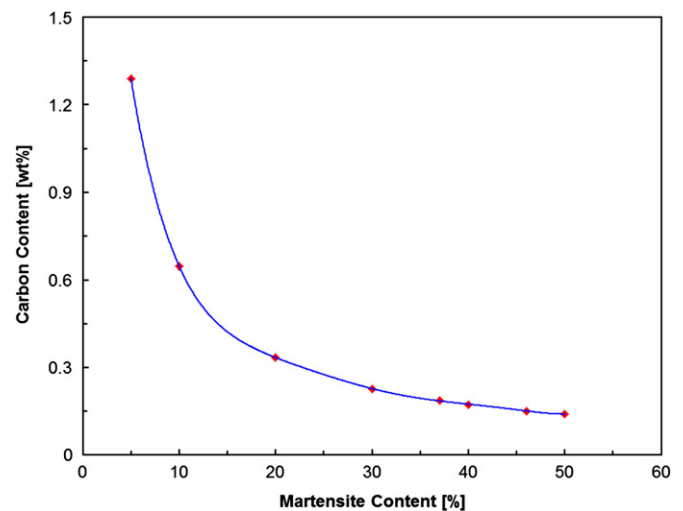
Fig. 4.1.3. Relation between the carbon content in martensite with the martensite phase fraction in studied DP600 steel.

Based on these results, an empirical relation is obtained between martensite fraction V_m (in volume %) of the DP600 steel and the ferrite grain size (in µm) as given in Eq. (4.1):

$$d_\alpha(\text{in } \mu m) = -0.046 \times V_m + 5.38 \tag{4.1}$$

Using ThermoCalc calculations, an empirical relationship was developed for the carbon content of ferrite and martensite fraction in the studied DP600 steel. Fig. 4.1.2 shows the carbon content (in wt%) in ferrite as a function of martensite volume fractions (in volume %). From this figure, it is observed that the carbon content in ferrite increases by increasing martensite content up to 8% and afterwards it starts decreasing with the increasing martensite fraction of DP600 steel. Therefore, the carbon content in ferrite can be described as a 6th-order polynomial function of martensite phase fraction (Eq. (4.2)).

$$\%C_{ss}^f = -7 \times 10^{-12} \times V_m^6 + 1 \times 10^{-9} \times V_m^5 - 1 \times 10^{-7} \times V_m^4$$
$$+ 5 \times 10^{-6} \times V_m^3 - 0.0001 \times V_m^2 + 0.001 \times V_m + 0.0048 \tag{4.2}$$

By combination of Eq. (2.1) (carbon mass balance equation) and Eq. (4.2), the carbon content of martensite can be identified in the
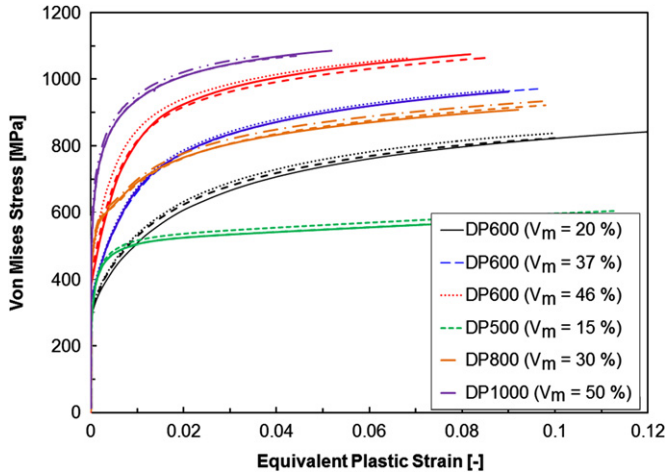
Fig. 4.2.1. Experimental flow curve of investigated DP steels with various chemistries and martensite phase fractions.
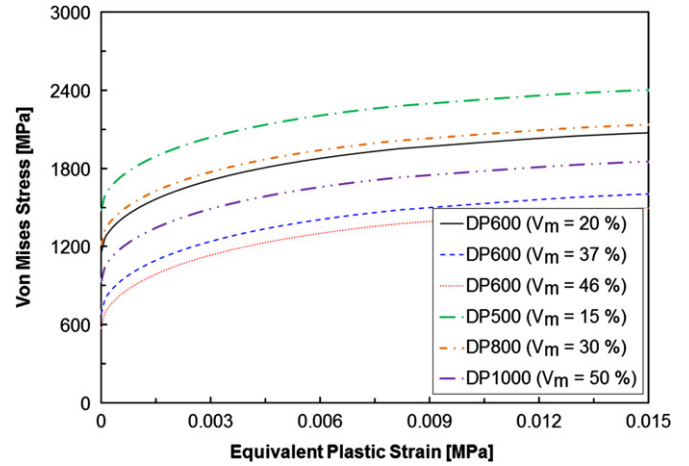

Fig. 4.3.2. Calculated von Mises stress—equivalent plastic strain responses of martensite for studied DP steels.
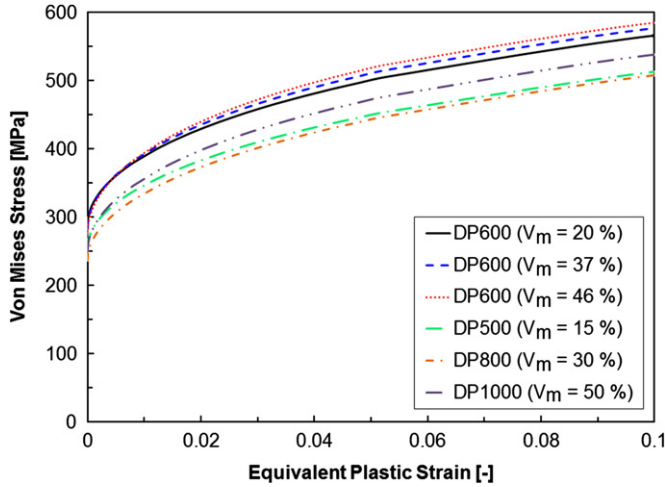
4.3. Flow curve of single phases

Rodriguez's approach [63], as discussed in Section 3.2, is used to develop the flow curve of ferrite at room temperature for each studied DP steel (Fig. 4.3.1). For the ferrite phase in DP600 annealed at different temperatures, the disparities between the flow curves are marginal. Fig. 4.3.1 also shows the calculated flow curve of ferrite in DP500, DP800 and DP1000 steels.

The martensitic flow curves are shown in Fig. 4.3.2. For DP600 steel, the dissimilarities between the flow curves of martensitic phases annealed at various temperatures are considerably significant in comparison with the ferrite flow curves. The calculated stress–strain behaviour of the martensite phases of the DP500, DP800 and DP1000 steels are also demonstrated in this figure. The increase of the strength of the martensite flow curve is primarily due to increase in the carbon content. The martensitic flow curve of the DP500 steel is greater than the DP600 steel due to the fact that the carbon content of martensite for the chemistry of the investigated DP500 steel is higher than the martensite carbon content of the studied DP600 steels with various amounts of martensite fraction in this research work. For the carbon content in martensite, please refer to Table 4.1.1, where the austenite carbon content is reported. (During cooling after intercritical annealing, the austenite transforms to martensite with the same carbon content).

4.4. Numerical tensile tests

Numerical tensile tests were carried out on the generated 2D and 3D RVEs of DP600 steel. The evolution of stress and strain in the RVEs can be obtained from these numerical tensile tests.

Fig. 4.4.1 illustrates the contour plot of von Mises stress and the equivalent plastic strain on microscale at $\varepsilon = 0.1$ for DP600 steel containing 20% martensite (the left-hand side figure shows von Mises stress distribution and the right-hand side figure demonstrates equivalent plastic strain distribution). In all situations, the formation of shear bands is noticed in 2D RVEs. The shear bands of the localised plastic strain in the ferrite are most likely exaggerated due to the plane strain condition. The direction of the localised plastic deformation is on average 45° to the tensile direction. High stresses up to 1700 MPa were noticed in the martensitic areas.

Von Mises stress and equivalent plastic strain were calculated for ferrite and martensite in any increment of deformation for both 2D and 3D models. Then, a computational first-order homogenisation by volume averaging was employed to obtain the true stress–true strain graph from the 2D and 3D RVE simulations [47].
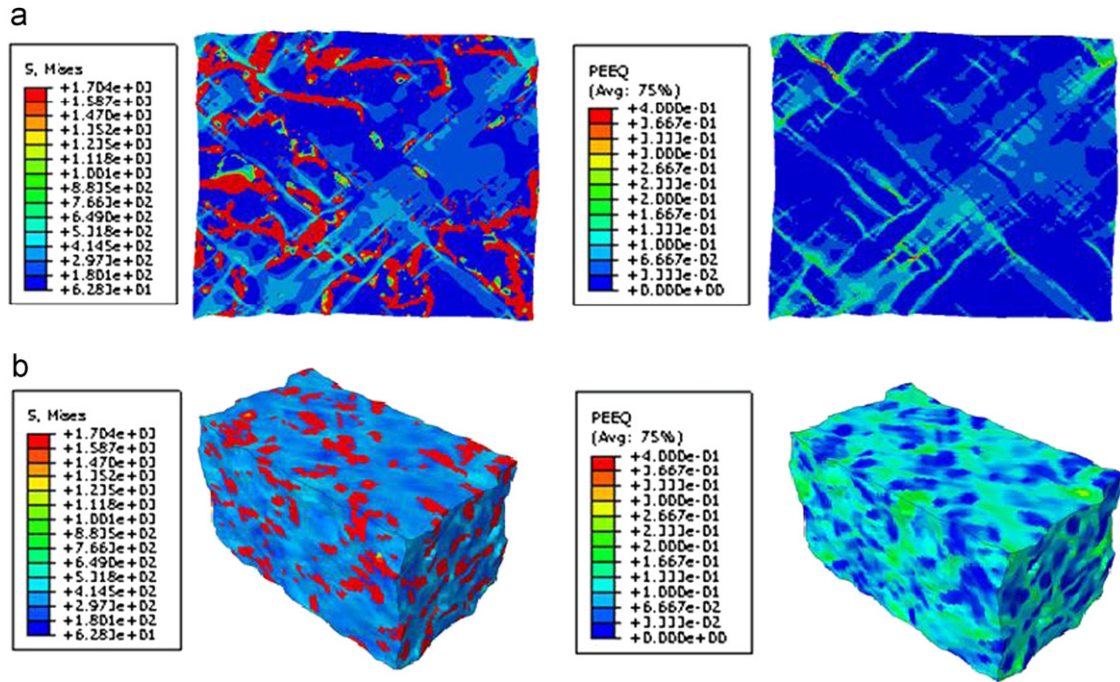

Fig. 4.3.1. Calculated von Mises stress—equivalent plastic strain responses of ferrite for studied DP steels.

studied DP600 steel with various martensite fractions ($V_m = 0$–50%). The calculated carbon content (in wt%) of martensite is shown in Fig. 4.1.3 as a function of martensite volume fractions (in volume %). As shown in this figure, the carbon content in martensite decreases with increasing martensite fraction of DP600 steel following the 6th-order polynomial function.

The empirical relation is obtained between carbon fraction (in wt%) in martensitic phase and martensite fraction V_m (in volume %) in the studied DP600 steel as given in Eq. (4.3):

$$\%C_{ss}{}^m = 3 \times 10^{-9} \times V_m{}^6 - 5 \times 10^{-7} \times V_m{}^5 + 4 \times 10^{-5} \times V_m{}^4$$
$$- 0.0017 \times V_m{}^3 + 0.0392 \times V_m{}^2 - 0.4857 \times V_m + 2.9273$$

(4.3)

4.2. Experimental tensile tests

The experimental flow curves for all studied DP steels are depicted in Fig. 4.2.1. For each condition, three tensile tests were performed and the results from all three tests are included in Fig. 4.2.1. As shown in this figure, the flow stress increases with the increase of the martensite fraction in every condition. Further, it can be concluded that the variation in flow curves for any specific martensite fraction is very small.

Fig. 4.4.1. Von Mises stress and equivalent plastic strain distribution on 2D and 3D RVE of DP600 steel with 20% martensite at $\varepsilon = 0.1$.
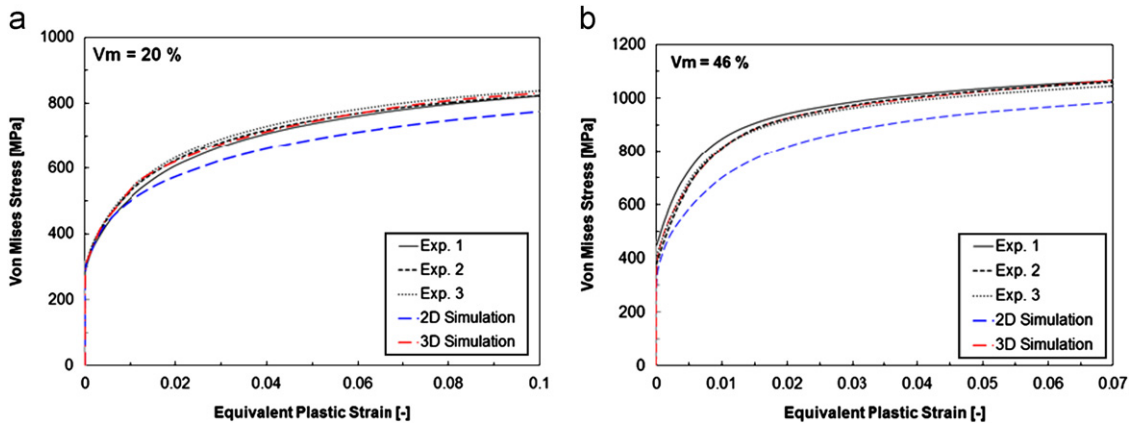

Fig. 4.4.2. Experimental and simulated flow curve of DP steel with (a) 20% and (b) 46% martensite.

A comparison between experimental and calculated true stress–true strain curves of the investigated DP600 steels with 20% and 37% martensite is demonstrated in Fig. 4.4.2. The results of finite element simulations using 2D and 3D approaches were compared with the experimental results in order to investigate the effect of dimensionality. It is evident that the flow curves of 3D simulation are much closer to those of the experimental flow curves compared to those of the 2D simulation in all investigated DP microstructures. It seems that the main reason for the deviation in the 2D simulation is the planar state of strain adopting on the calculations. During the real tensile test, the specimen deforms three dimensionally; therefore, the deviation should appear. The deviation of 2D prediction from the experimental results increases by increasing the martensite fraction in DP600 steel.

4.5. Determination of correlation between simulated 2D and 3D flow curves

DP600 steel with 20%, 37% and 46% martensite fraction has been developed experimentally by laboratory intercritical annealing. Additionally, the flow behaviour of DP steels with 0%, 5%, 10%, 15%, 25%, 30%, 40% and 50% martensite was studied numerically to develop an accurate correlation between 2D and 3D calculations. For creating a series of 2D RVEs with systematic variation of martensite fraction, special portions containing above the prescribed fraction of martensite were examined in micrographs. A series of 3D RVEs were also generated with the same martensite fractions from 0% to 50%. The ferrite grain size and carbon content of ferrite and martensite were calculated by employing the Eqs. (4.1) and (4.3) respectively. Based on these data, flow curves of ferrite and martensite were identified according to the variation of martensite content using a dislocation-based model (Section 3.2). The flow curves for ferrite and martensite are represented in Fig. 4.5.1. The differences between the flow curves of martensitic phases are remarkably higher as compared to the flow curves of ferrite.

The results of simulations for RVE with 0%, 10%, 30% and 50% martensite fraction are demonstrated in Fig. 4.5.2. It is evident that the flow curves of 2D and 3D simulations are overlapped for
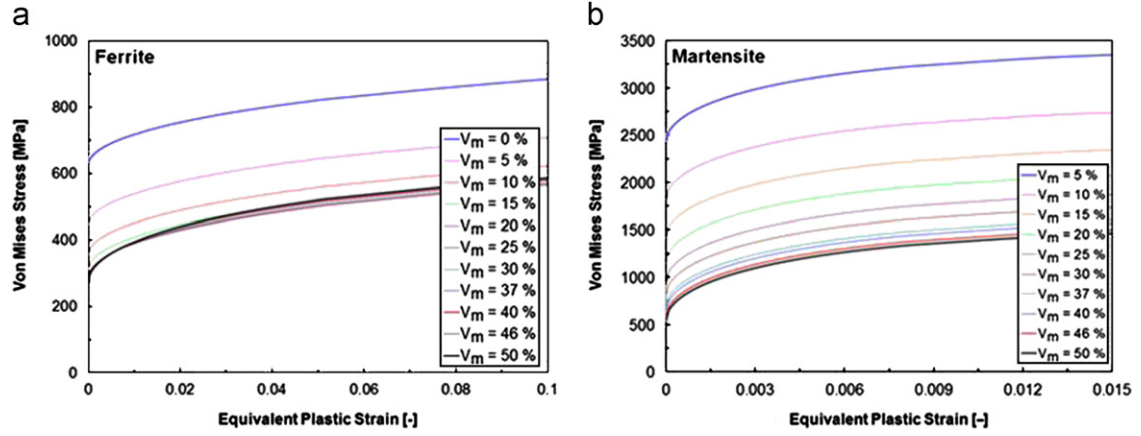
Fig. 4.5.1. Flow curves of (a) ferrite and (b) martensite for DP600 steel with various martensite phase fractions.
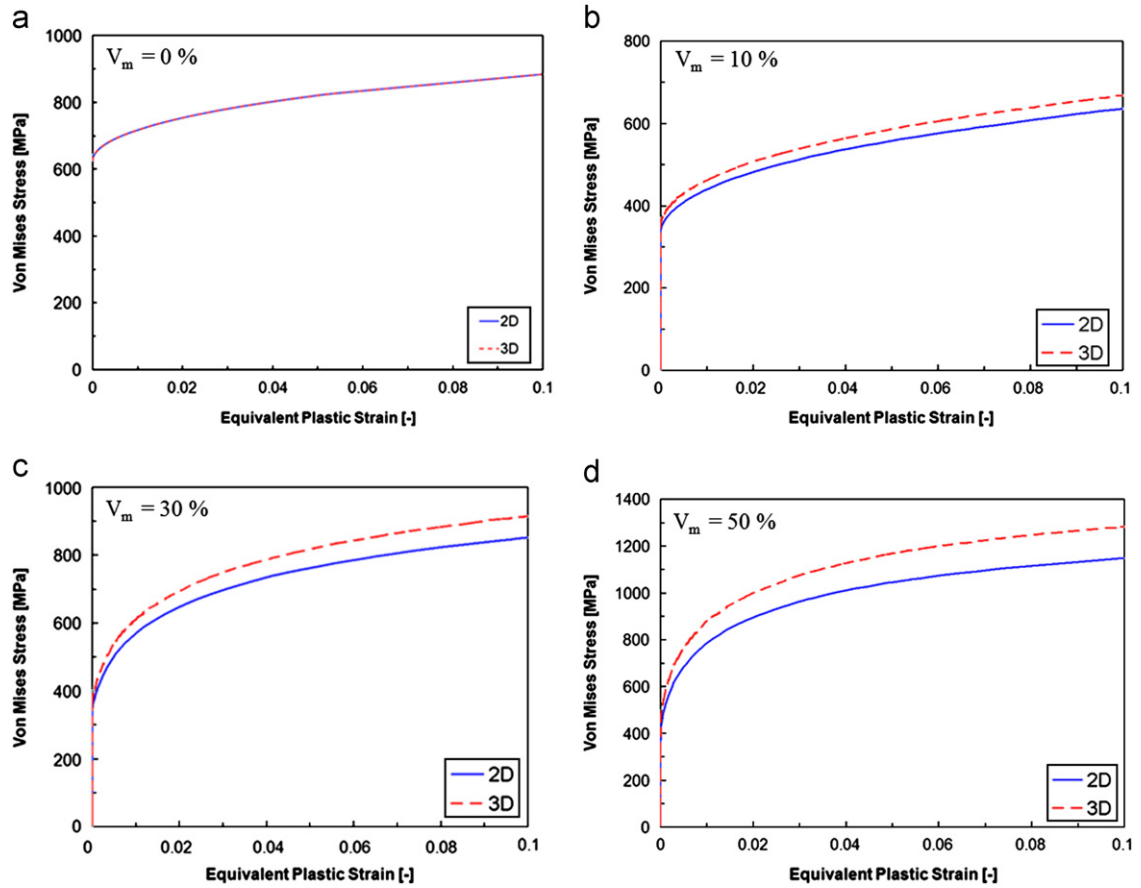

Fig. 4.5.2. 2D vs. 3D comparison of simulated flow curves of DP steels with (a) 0%, (b) 10%, (c) 30% and (d) 50% martensite fractions.

the $V_m=0\%$ condition. The ratio of σ_{3D}/σ_{2D} increases by increasing the martensite fraction from 5% to 50%.

The ratio of σ_{3D}/σ_{2D}, which is introduced as a correlation factor, was determined from the predicted flow curves of the 2D and 3D RVE models with martensite fractions V_m varying from 0% to 50% at equivalent plastic strains ε_{eq}^p varying from 0 to 0.1, as illustrated in Fig. 4.5.3. The results indicated that at $\varepsilon_{eq}^p=0$ the σ_{3D}/σ_{2D} ratio increases from 1 to 1.34 when the martensite fraction increases from 0% to 50%; however, at ($\varepsilon_{eq}^p=50\%$), σ_{3D}/σ_{2D} enhances from 1 to 1.86. It is evident that the deviation between the predicted flow stresses by 2D and 3D models is intensified by increasing the martensite fraction, as shown in Fig. 4.5.3. Subsequently, σ_{3D}/σ_{2D} was developed

as a function of the martensite fraction and equivalent plastic strain using MATLAB software, which is shown in Eq. (4.4).

$$\begin{aligned}
\sigma_{3D}/\sigma_{2D} = {} & 2 \times 10^{-4} \times (\varepsilon_{eq}^p)^2 \times V_m^3 - 1 \times 10^{-7} \times (\varepsilon_{eq}^p) \times V_m^3 \\
& + 1 \times 10^{-7} \times V_m^3 + 0.0218 \times (\varepsilon_{eq}^p)^2 \times V_m^2 \\
& - 0.0015 \times (\varepsilon_{eq}^p) \times V_m^2 + 7 \times 10^{-5} \times V_m^2 + 0.18 \\
& \times (\varepsilon_{eq}^p)^2 \times V_m + 0.007 \times (\varepsilon_{eq}^p) \times V_m + 0.0036 \\
& \times V_m \times (\varepsilon_{eq}^p)^2 + 1
\end{aligned}$$

(4.4)

4.6. Generalisation

The correlation factor Eq. (4.4) was developed for a series of DP600 steels with varying martensite fractions but the same chemistry. As a validation, now this concept will be applied for DP grades with different chemistries and martensite fractions. Uniaxial numerical tensile tests were performed on the 2D- and 3D-generated RVEs for DP500 ($V_m=15\%$), DP600 ($V_m=20\%$), DP800 ($V_m=30\%$) and DP1000 ($V_m=50\%$). The results of finite element simulations using 2D and 3D approaches were compared with the experimental results in Fig. 4.6.1. The comparison between experimental and numerical results revealed that the

3D simulations gave better agreement with the experimental results as compared to the 2D simulations in all conditions. Further, the difference between the predicted behaviour from the 2D calculation and 3D calculation is considerably higher than the scatter in the experimental results.

Fig. 4.6.2 shows the comparison between the calculated σ_{3D}/σ_{2D} from the developed correlation factor and identified σ_{3D}/σ_{2D} from the 2D and 3D RVE calculations for DP500, DP600, DP800 and DP1000 steels at $\varepsilon_{eq}^p=0$ and 0.1. The theoretical correlation obtained from Eq. (4.4) matches perfectly with the one obtained from the simulated von Mises stresses from 2D and 3D approaches for all investigated DP steels.
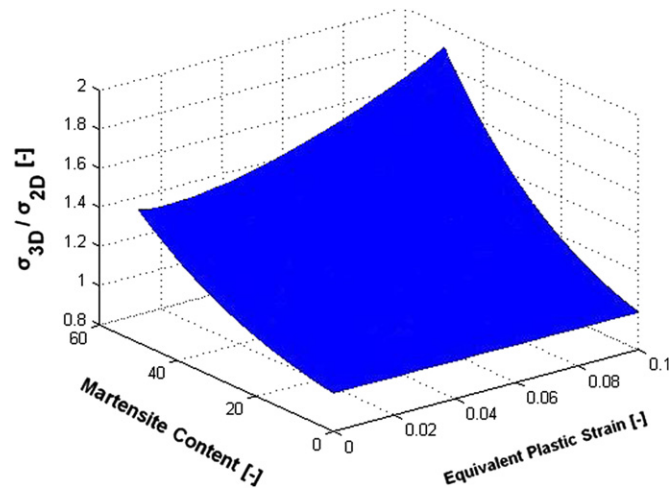
5. Conclusions

2D RVE is generated based on real micrographs and can involve all microstructural features in the calculations. But 3D RVE is created using statistical algorithms. The much shorter calculation time is also another major advantage of 2D calculations. The specimen deforms three-dimensionally in the uniaxial tensile test; however, 2D modelling approaches are not able to predict the flow curve of material precisely. Therefore, the predicted flow curves of 2D modelling should be correlated to the 3Ds by introducing a correlation factor in order to study the effect of microstructural features on the mechanical properties of DP steel precisely. This function is introduced as σ_{3D}/σ_{2D} based on the 2D and 3D RVE calculations for DP600 steels with various martensite phase fractions ($V_m=0–50\%$) at different equivalent plastic strains varying from $\varepsilon_{eq}^p=0–0.1$. The developed correlation factor is a polynomial equation regarding martensite fraction and equivalent plastic strain. The calculated result from this approach
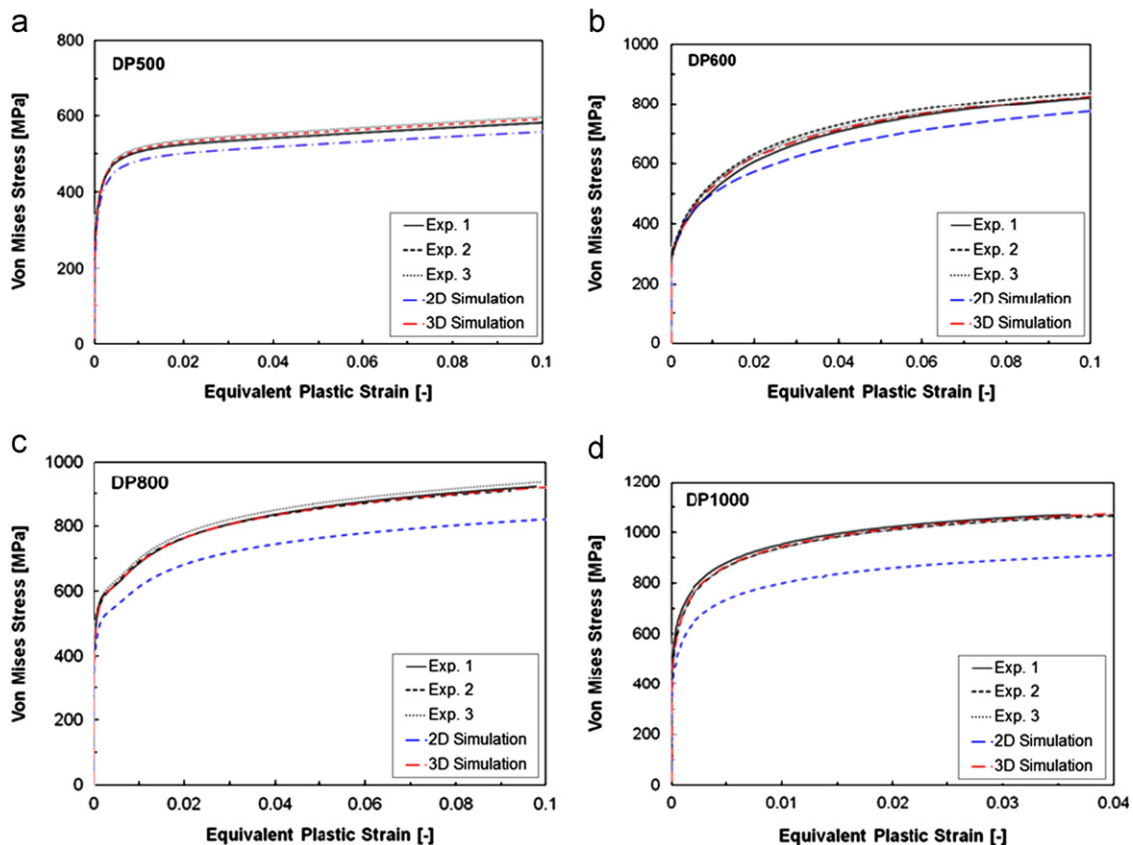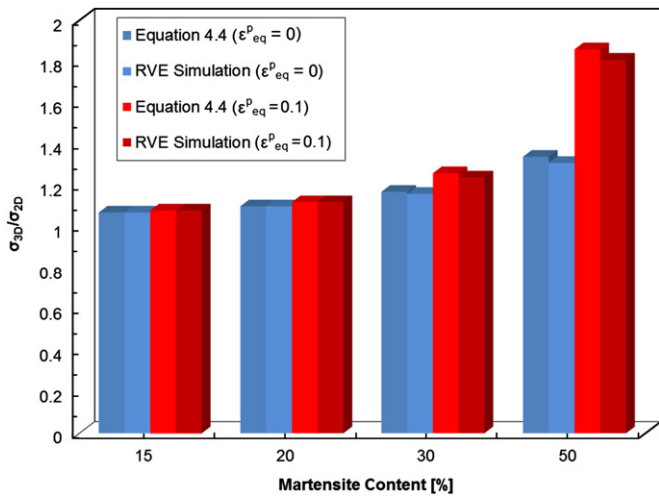

Fig. 4.5.3. 2D–3D flow curve correlation factor for studied DP600 steel.

Fig. 4.6.1. Experimental and simulated flow curve of (a) DP500, (b) DP600, (c) DP800 and (d) DP1000 steels.

Fig. 4.6.2. Comparison between σ_{3D}/σ_{2D} identified from the developed correlation factor and RVE calculations for DP500, DP600, DP800 and DP1000 steels at $\varepsilon_{eq}^{p}=0$ and 0.1.

at different equivalent plastic strains is in good agreement with the obtained results (σ_{3D}/σ_{2D}) from simulations for different DP steel grades. Therefore, the developed approach can be held for DP steels with various chemistries, strength levels and martensite fractions.

Acknowledgements

References

[1] WorldAutosteel, Ultra-Light Steel Auto Body—Advanced Vehicle Technology (ULSABAVC) Programme, www.elsab.org, Overview Report, January 2002.
[2] M. Pfestorf, The application of multiphase steel in the Body-in-White, Great Designs in Steel seminar, BMW group, 2005.
[3] H. Qu, Advanced High Strength Steel Through Paraequilibrium Carbon Partitioning and Austenite Stabilization, Master Thesis, 2011.
[4] ULSAB-AVC-PES Engineering Report, October 2001.
[5] B.K. Zuidema, S.G. Denner, B. Engl, J. Sperle, New High Strength Steels Applied to the Body Structure of ULSAB-AVC, Society of Automotive Engineers, 2011, pp. 984–992.
[6] J.M. Rigsbee, P.J. Van der Arend, Formable HSLA and Dual-phase Steels, TMS-AIME, Warrendale, PA, 1979, pp. 56–86.
[7] G.R. Speich, R.L. Miller, Structure and Properties of Dual-Phase Steels, TMS-AIME, Warrendale, PA, 1979, pp. 145–182.
[8] M.S. Rashid, Annu. Rev. Mater.Sci. 11 (1981) 245–266.
[9] G.R. Speich, Fundamental of Dual-Phase Steels, TMS-AIME, Warrendale, PA, 1981, pp. 3–45.
[10] N.K. Balliger, T. Gladman, Met. Sci. 15 (1981) 95–108.
[11] C.A.N. Lanzillotto, F.B. Pickering, Met. Sci. 16 (1982) 371–382.
[12] J.Y. Koo, M.J. Young, G. Thomas, Metall. Trans. A 11 (1980) 852–854.
[13] F.B. Pickering, Constitution and Properties of Steels, Wiley-VCH., 1992, pp. 77–79.
[14] T. Gladman, The Physical Metallurgy of Microalloyed Steels, The Institute of Metals, London, 1997, pp. 325–336.
[15] A. Bag, K.K. Ray, E.S. Dwarakadasa, Metall. Mater. Trans. A 30 (1999) 1193–1202.
[16] N.J. Kim, G. Thomas, Metall. Trans. A 12 (1981) 483–489.
[17] F.B. Pickering, Advances in the Physical Metallurgy and Applications of Steels, The Metals Society, 1981, pp. 5–25.
[18] A.M. Sherman, R.G. Davies, Int. J. Fatigue 3 (4) (1981) 195–198.
[19] D.L. Bourell, A. Rizk, Acta Metall. 31 (1983) 609–617.
[20] U. Liedl, S. Traint, E.A. Werner, Comput. Mater. Sci. 25 (2002) 122–128.
[21] W.C. Leslie, The Physical Metallurgy of Steels, McGraw-Hill, New York, 1981, pp. 216–23.
[22] A.S. Khan, M. Baig, S.H. Choi, H.S. Yang, X. Sun, Int. J. Plasticity 30–31 (2012) 1–17.
[23] A.S. Khan, R. Liang, Int. J. Plasticity 15 (1999) 1089–1109.
[24] A.S. Khan, Y.S. Suh, R. Kazmi, Int. J. Plasticity 20 (2004) 2233–2248.
[25] A.S. Khan, R. Kazmi, B. Farrokh, Int. J. Plasticity 23 (2007) 931–950.
[26] S.A. Asgari, P.D. Hodgson, C. Yang, B.F. Rolfe, Comput. Mater. Sci. 45 (2009) 860–866.
[27] A. Ramazani, K. Mukherjee, U. Prahl, W. Bleck, Comput. Mater. Sci. 52 (1) (2012) 46–54.
[28] C. Thomser, V. Uthaisangsuk, W. Bleck, Steel Res. Int 80 (8) (2010) 582–587.
[29] C. Thomser, U. Prahl, H. Vegter, W. Bleck, Comput. Methods Mater. Sci. 7 (1) (2007) 42–46.
[30] U. Prahl, S. Papaefthymiou, V. Uthaisangsuk, W. Bleck, J. Sietsma, S. van der Zwaag, Comput. Mater. Sci. 39 (2007) 17–22.
[31] V. Uthaisangsuk, U. Prahl, W. Bleck, Comput. Mater. Sci. 43 (2008) 27–35.
[32] F.M. Al-Abbasi, J.A. Nemes, Int. J. Mech. Sci. 45 (2003) 1449–1465.
[33] W. Bleck, W. Kaluza, K. Papamantellos, Proceedings of the 10th International Symposium Metallography, April 1998, pp. 88–92.
[34] S. Ghosh, J. Bai, D. Paquet, J. Mech. Phys. Solids 57 (2009) 1017–1044.
[35] National Institute of Standards and Technology (USA), Object-Oriented Finite Element Program, Version 2.4, 2007, http://www.ctcms.nist.gov/oof/.
[36] S.H. Xia, J.T. Wang, Int. J. Plasticity 26 (2010) 1442–1460.
[37] H. Lim, M.G. Lee, J.H. Kim, B.L. Adams, R.H. Wagoner, Int. J. Plasticity 27 (2011) 1328–1354.
[38] N. Srivastava, G.J. Weng, Int. J. Plasticity 23 (2007) 1860–1873.
[39] J.H. Kim, M.G. Lee, D. Kim, D.K. Matlock, R.H. Wagoner, Mater. Sci. Eng., A 527 (2010) 7353–7363.
[40] X. Sun, K.S. Choi, W.N. Liu, M.A. Khaleel, Int. J. Plasticity 25 (2009) 1888–1909.
[41] C. Thomser, Modelling of the Mechanical Properties of Dual Phase Steels based on Microstructure, Ph.D. Thesis, RWTH-Aachen, Germany, 2009.
[42] V. Tvergaard, Int. J. Fract. Mech. 17 (1981) 389–407.
[43] S. Socrate, M.C. Boyce, J. Mech. Phys. Solids 48 (2000) 233–273.
[44] Y. Huang, A.J. Kinloch, J. Mater. Sci. 27 (1992) 2753–2762.
[45] M. Danielsson, D.M. Parks, M.C. Boyce, J. Mech. Phys. Solids 50 (2) (2002) 351–379.
[46] N. Ishikawa, D.M. Parks, S. Socrate, M. Kurihara, Iron Steel Inst. Jpn. Int. 40 (11) (2000) 1170–1179.
[47] F. Alabbasi, Micromechanical Modelling of Dual Phase Steels, Ph.D. Thesis, McGill University, Montreal, Canada, 2004.
[48] M. Calcagnotto, D. Ponge, E. Demir, D. Raabe, Mater. Sci. Eng. A 527 (2010) 2738–2746.
[49] T. Iung, M. Grange, Mater. Sci. Eng. A 201 (1995) L8–L11.
[50] L. Durand, C. Thomas de Montpréville, Res. Mechanica 29 (1990) 257–285.
[51] J.B. Leblond, G. Mottet, J.C. Devaux, J. Mech. Phys. Solids 34 (1992) 335–342.
[52] A.C. Lewis, A.B. Geltmacher, Scripta Mater. 55 (2006) 81–85.
[53] A.C. Lewis, K.A. Jordan, A.B. Geltmacher, Metall. Mater. Trans. A 39 (2008) 1109–1117.
[54] N. Chawla, R.S. Sidhu, V.V. Ganesh, Acta Mater. 54 (2006) 1541–1548.
[55] V. Uthaisangsuk, Microstructure Based Formability modelling of Multiphase Steels, Ph.D. Thesis, RWTH-Aachen, Germany, 2009.
[56] W. Kaluza, Modellierung der mechanischen Eigenschaften und der lokalen Dehnung von Dualphasen-Stählen, Ph.D. Thesis, RWTH-Aachen, Germany, 2003.
[57] T. Mori, K. Tanaka, Acta Metall. 21 (1977) 571–574.
[58] J. Rudnizki, Through-Process Model for the Microstructure of Dual-Phase Steel, Ph.D. Thesis, RWTH-Aachen, Germany, 2011.
[59] J.H. Kim, D. Kim, F. Barlat, M.G. Lee, Mater. Sci. Eng. A 539 (2012) 259–270.
[60] J.R. Mayeur, D.L. McDowell, Int. J. Plasticity 23 (2007) 1457–1485.
[61] V.G. Kouznetsova, Computational Homogenization for the Multi-Scale Analysis of Multiphase Materials, Ph.D. Thesis, Technical University Eindhoven, The Netherlands, 2002.
[62] M.G. Lee, H. Lim, B.L. Adams, J.P. Hirth, R.H. Wagoner, Int. J. Plasticity 26 (2010) 925–938.
[63] R.M. Rodriguez, I. Gutierrez, Mater. Sci. Forum 426–432 (2003) 4525–4530.
[64] Y. Bergström, Mater. Sci. Eng. 5 (4) (1970) 193–200.
[65] Y. Estrin, H. Mecking, Acta Metall. 32 (1) (1984) 57–70.
[66] J.G. Sevillano, Mater. Sci. Technol. 6 (1993).
[67] O. Bouaziz, P. Buessler, Rev. Metall.-CIT 99 (2002) 71–77.
[68] M. Mazinani, Deformation and Fracture Behaviour of a Low Carbon Dual-Phase Steel, Ph.D. Thesis, The University of British Columbia, Vancouver, Canada, 2006.